Nuclear Instruments and Methods in Physics Research B 541 (2023) 56–60

Contents lists available at ScienceDirect

Nuclear Inst. and Methods in Physics Research, B

journal homepage: www.elsevier.com/locate/nimb

Recent progress in the construction of KoBRA for low-energy nuclear physics experiments

K. Tshoo [a,*], S.J. Pyeun [a], K.B. Lee [a], C. Akers [a], J. Park [b], M.S. Kwag [a], M. Kim [a], J.C. Kim [a], D.G. Kim [a,c], Y.K. Kim [c], C. Ham [a], T. Shin [a], S. Lee [a], S. Ahn [d], J.W. Hwang [d], D.S. Ahn [d], D.H. Kim [d], K.I. Hahn [d], M. Kwon [a]

[a] Rare Isotope Science Project, Institute for Basic Science, Daejeon 34000, Republic of Korea
[b] Korea Atomic Energy Research Institute, Daejeon 34057, Republic of Korea
[c] Department of Nuclear Engineering, Hanyang University, Seoul 133-791, Republic of Korea
[d] Center for Exotic Nuclear Studies, Institute for Basic Science, Daejeon 34126, Republic of Korea

ARTICLE INFO

Keywords:
Rare isotope science project
RAON
KoBRA
Recoil spectrometer
Rare isotope production

ABSTRACT

A multi-purpose experimental instrument, called as KoBRA (Korea Broad acceptance Recoil spectrometer and Apparatus), has been constructed for low-energy nuclear physics experiments at RAON (Rare Isotope Accelerator complex for ON-line experiments), and is being prepared in order to produce rare isotope beams at an energy of about 20 MeV/nucleon during the first beam commissioning phase. A test was performed to measure the positions of ^{4}He ions at the dispersive and achromatic foci of KoBRA using an ^{241}Am α-source placed at the production target position, so as to examine the momentum dispersion and ion beam transport. We report on the results of the test and the detailed design of KoBRA including ion optics, together with the status of detectors for particle identification of rare isotopes.

1. Introduction

KoBRA [1] is a multi-purpose experimental instrument using stable or rare isotope (RI) beams for low-energy nuclear physics experiments at the Korean heavy ion accelerator facility RAON [2–6]. The stable ions are delivered to KoBRA after acceleration by SCL3 (superconducting linear accelerator 3) up to a few tens of MeV/nucleon. KoBRA will be employed to produce and separate RI beams using a stable ion beam with a production target. An ISOL (Isotope Separation On-Line) facility constructed at RAON will also provide RI beams to KoBRA for nuclear physics and nuclear astrophysics experiments, where SCL3 is used as a post-accelerator of the ISOL facility. The potential physics program using the RI beams produced at RAON has been discussed in Refs. [7–10].

A schematic view of KoBRA is shown in Fig. 1. KoBRA consists of a beam swinger used to control the incident angle of the primary beam onto the production target, a production target chamber, a primary beam dump chamber, two curved-edge bending magnets, fifteen quadrupole magnets, two hexapole magnets, three focal plane chambers, and one velocity filter (Wien filter). The specification of KoBRA is summarized in Table 1.

KoBRA was installed on June of 2021 except for the Wien filter, and the area upstream of F2 was radiation shielded with concrete blocks. Since the Wien filter is being manufactured at present [11], a beam pipe was installed in its place instead. Hence, the first beam commissioning of KoBRA will be performed without the Wien filter.

An ^{40}Ar beam will be used as a primary beam for the RI beam production, during the first beam commissioning of KoBRA. Since the $^{40}Ar^{9+}$ beam can be accelerated by SCL3 up to about 27 MeV/nucleon, an RI beam can be produced via the multi-nucleon transfer reactions described as in Refs. [12–15].

The secondary beam following reactions of the ^{40}Ar primary beam of energy about 20 MeV/nucleon with the production target can be identified particle-by-particle by employing the $B\rho$-TOF-ΔE technique. The magnetic rigidity ($B\rho$) is determined from the position measurement at the dispersive focus F1. The time-of-flight (TOF) of the secondary beam is measured between the double achromatic foci F2 and F3 with thin plastic scintillator detectors. The energy loss (ΔE) is measured using a thin silicon detector placed at F2 or F3. We have a plan to perform an experiment to measure the production cross sections of secondary beams with the commissioning beam.

In this paper, we report on the recent progress in the construction of KoBRA. The detailed design parameters of KoBRA are described along with the present construction status. The result of an α-particle transport test of KoBRA is also reported. A comparison of the measured

* Corresponding author.
E-mail address: tshoo@ibs.re.kr (K. Tshoo).

https://doi.org/10.1016/j.nimb.2023.05.005
Received 26 January 2023; Received in revised form 28 April 2023; Accepted 2 May 2023
Available online 15 May 2023

Table 1
Specification of KoBRA. The first order magnification and dispersion are denoted by M and D, respectively.

Magnetic rigidity	0.25 - 3.0 Tm
Horizontal angular acceptance	±40 mrad
Vertical angular acceptance	±100 mrad
Momentum acceptance	±4%
Momentum resolving power $D_p/2M_x$ at F1	2092
Mass resolving power $D_m/2M_x$ at F3	790[a]
Tilting angle of ion beam on the production target	±12°[b]

[a]This value is for $^{66}Se^{19+}$ at an energy of 1 MeV/nucleon with zero momentum dispersion at F3. The mass resolving power depends on the energy and the mass-to-charge ratio.
[b]Maximum angle for 3 Tm magnetic rigidity.

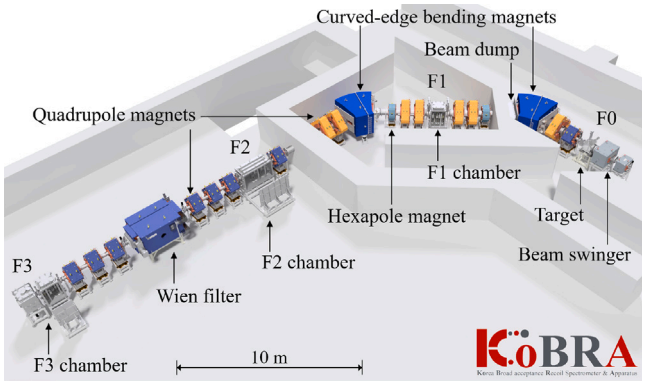

Fig. 1. Schematic view of KoBRA.

Table 2
Magnification and dispersion of KoBRA for each focus.

	M_x	M_y	D_p
Dispersive focus F1	0.98	−10.3	4.10 m
Double achromatic focus F2	−2.60	3.16	0.0 m
Double achromatic focus F3	3.30	3.80	0.0 m

and simulated position distributions of the α-particles is indicative of KoBRA successfully operating in terms of ion beam transport. The designed momentum dispersion at F1 was confirmed from the position measurement.

2. Ion optical design of KoBRA

KoBRA is a two-bend achromatic spectrometer consisting of two 45 degree bending magnets, combined with the Wien filter. Quadrupole triplet magnets are located both upstream and downstream of the Wien filter. There are one momentum dispersive focus (F1) and two double achromatic foci (F2 and F3) as shown in Fig. 1. The F3 focus can be used as a mass dispersive focus with the Wien filter switched on. All the foci have satisfied the point-to-point focus conditions with zero angular dispersion in the first order ion optics, in both vertical and horizontal directions. A homogeneous or curved energy degrader can be inserted at F1 for further separation by employing the energy-loss achromat technique. The first order horizontal and vertical magnifications (M_x and M_y) and horizontal momentum dispersion (D_p) are listed in Table 2. The magnifications at F2 and F3 are changed when the homogeneous energy degrader is used with an additional ion-optics tune to give a double achromatic focus at F2.

The ion optical design of KoBRA was performed using the code COSY INFINITY [16]. The effective field lengths and the fringe field distributions of magnets were calculated using the three dimensional finite-element code OPERA3D, and reflected in the ion optics calculation. The calculated three dimensional magnetic field maps of the quadrupole and hexapole magnets were decomposed into the leading

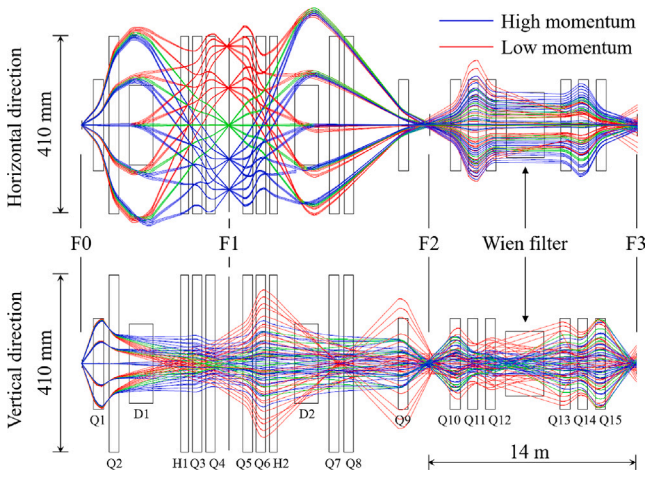

Fig. 2. Horizontal and vertical rays of KoBRA with the Wien filter switched off calculated from the fifth order ion-optics calculation. Beam trajectories are shown with an angular spread of ±40 mrad (±100 mrad) and beam size of ±1 mm in the horizontal (vertical) plane with a momentum spread of ±4%.

and the higher-order pseudo terms as described in Ref. [17]. The leading terms extracted from the three dimensional magnetic field maps were used for the ion optics calculation. Fig. 2 shows the selection of rays of a fifth order ion optics calculation with the Wien filter switched off.

Since KoBRA is a large acceptance spectrometer, the minimization of the high order aberrations was one of main tasks for the ion optical design. We introduced the two curved-edge bending magnets to minimize the high order aberrations up to fourth order, combined with the two hexapole magnets. Such a curved-edge bending magnet has been used in the SHARAQ spectrometer [18–20] and the recoil mass separator SECAR [21,22], which is useful to eliminate higher-order terms without multipole magnets. The entrance and exit curves of the bending magnets of KoBRA are described by fourth order polynomial functions. The details of the bending magnet will be described in the following section.

3. Magnets and wien filter of KoBRA

The detailed design parameters of the magnets and Wien filter are listed in Table 3. The beam swinger consists of two rectangular dipole magnets (SW1 and SW2). The direction of tilting angle on the target is variable by using bipolar power supplies. The relative field homogeneity of SW1 and SW2 is 10^{-3} in the horizontal good field region (HGFR) within 10 - 100% field excitation range. The tails of the fringe fields are cut off by field clamps on both the entrance and the exit sides.

Small and large aperture quadrupoles magnets (SQ and LQ), as well as the hexapole magnet (H) were designed in accordance with the ion optical design. The aperture radii (R_{bore}) of SQ, LQ, and H are 105, 205, and 205 mm, respectively. The effective field lengths (L_{eff}) of SQ, LQ, and H are 668.5, 640.5, and 527.5 mm, respectively. The quadrupole and hexapole magnets were designed so that the variation of the L_{eff} is ±0.5 mm in 2 - 100% field excitation range.

The bending angle (ϕ) and bending radius (ρ) of the curved-edge bending magnets (D1 and D2) were determined to be 45° and 2 m, respectively, from the ion optics. The relative field homogeneity of D1 and D2 is 2×10^{-4} in a magnetic field range of $0.125 \leq B \leq 1.5$ T. The shapes of the pole face perpendicular to the beam axis are described by the fourth order polynomial functions mentioned earlier, and were carefully determined to minimize the high order aberrations in the ion optical design taking into account the fringe field distributions of all the magnets. Fig. 3 shows a photograph of the pole piece of D1. The

Table 3
Design parameters of the magnets and Wien filter for KoBRA. The maximum magnetic field strength and the full gap are denoted by B_{max} and g, respectively. L_{yoke} is a length of the return yoke along the beam direction.

	B_{max} (T)	V_{nom} (kV)	g (mm)	R_{bore} (mm)	L_{eff} (mm)	L_{yoke} (mm)	ϕ (°)	ρ (m)	HGFR (mm)	VGFR (mm)
SW1	1.20		70		550.8	534.0			130	
SW2	1.51		60		857.0	836.0			260	
SQ	0.80[a]			105	668.5	592.0				
LQ	0.70[a]			205	640.5	496.0				
H	0.25[a]			205	527.5	428.0				
D1, D2	1.50		184		1570.8		45.0	2.0	400	
WF	0.20	±150	150[b]		2500.0	2380.0			150	100

[a]Maximum field strength at pole tip.
[b]Full gap between electrodes.

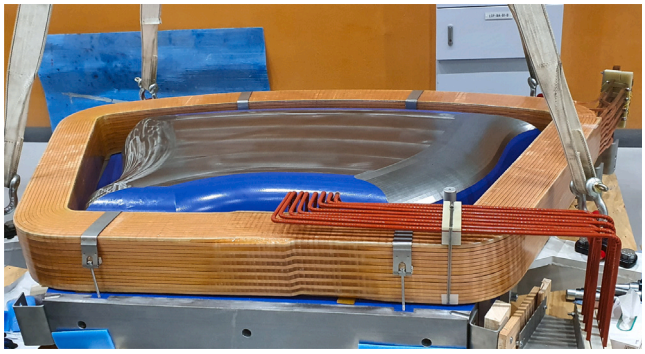

Fig. 3. Photograph of the pole piece of the curved-edge bending magnet D1. The shapes of the effective field boundaries on the entrance and exit pole faces are expressed with fourth order polynomial functions.

Rogowski function [23] was introduced on all the sides of the pole piece in order to reduce field saturation. The Rogowski shape provides better field saturation properties than the round shape, reducing the field strength dependence of the effective field boundary curve. The tails of the fringe fields are cut off by the field clamps.

The Wien filter (WF) is a device to select the velocity of charged particle with perpendicularly oriented electric and magnetic fields. The inside view of the Wien filter is shown in Fig. 4. The effective field length of the Wien filter was determined to be 2.5 m with a 150 mm full gap between its electrodes. The nominal electric potential (V_{nom}) on the electrode is ±150 kV corresponding to the electric field strength of 2 kV/mm. The dipole magnet can be excited up to 0.2 T. The horizontal and vertical good field regions (HGFR and VGFR) are 150 and 100 mm, respectively. The relative homogeneity of magnetic and electric fields is 5×10^{-4} for both HGFR and VGFR. The design concept of the Wien filter is similar with that of SECAR [21,22].

4. Installation of KoBRA

The weight of the curved-edge bending magnet is about 50 tons. Since the lifting capacity of the overhead crane in the experimental hall is 10 tons, it was segmented into several pieces weighing less than 10 tons, and delivered to the experimental hall of RAON. All the magnets were aligned with a tolerance of less than 100 μm after the fabrication of KoBRA. The radiation shielding concrete blocks with a thickness of about 0.8 m were carefully mounted around KoBRA during about two months after the alignment. The power supplies of the magnets were installed in the basement of the experimental hall. The power and control cables and the coolant hoses for KoBRA were laid on cable trays, and connected to each device. The detectors were mounted and aligned in the vacuum chambers. The signal and high voltage cables for the detectors were connected to NIM and VME electronics for signal processing. A control room was constructed in the basement. KoBRA can be monitored and controlled in the control room, using the TCP/IP protocol via an Ethernet connection. Fig. 5 shows photographs of KoBRA after installation.

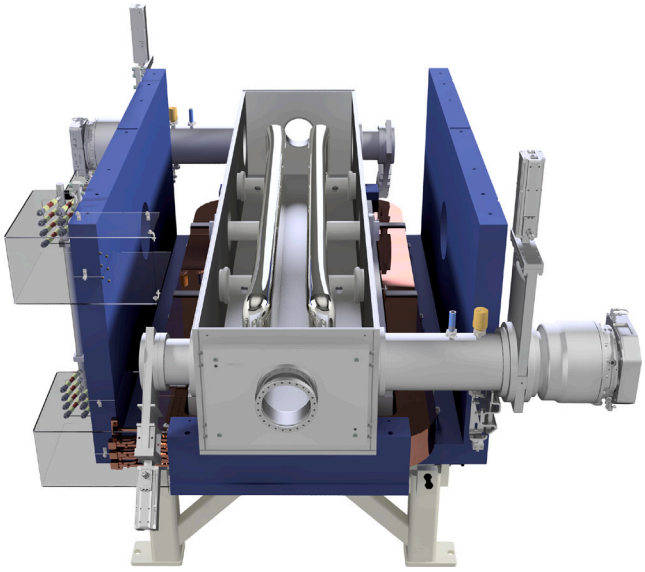

Fig. 4. Inside view of the Wien filter of KoBRA. The effective length of both electric and magnetic fields is 2.5 m.

Fig. 5. Photographs of KoBRA. (top) Photograph around the production target. (middle) Photograph around the F1 chamber. (bottom) Photograph around the F3 chamber.

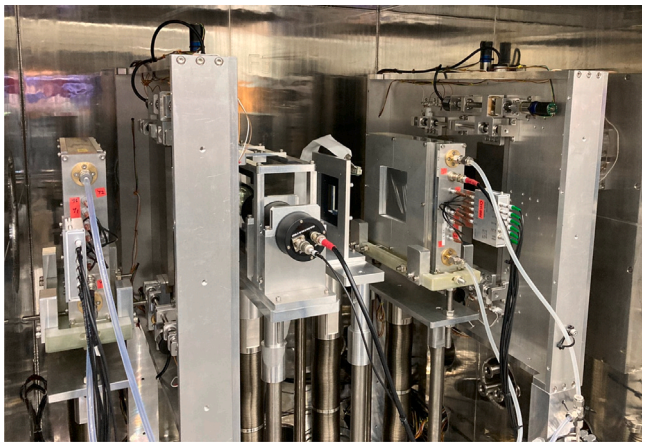

Fig. 6. Photograph of inside of the F3 chamber. The plastic detector, silicon detector, and small PPAC were installed between the slits.

5. Charged particle detectors for particle identification

We have developed multiple parallel plate avalanche counters (PPAC), two plastic scintillator detectors, and two silicon detectors for the position, the timing, and the energy loss measurements, respectively. A large PPAC with 40 × 20 cm^2 active area reported in Ref. [24] was installed in the F1 chamber for the position measurement. An additional large PPAC can be installed in the chamber for angle measurement. Two small PPACs with 10 × 10 cm^2 active areas [25] were installed in both F2 and F3 chambers for the position and angle measurements. Two 50 μm-thick plastic scintillators with 10 × 10 cm^2 area were mounted in both the F2 and F3 chambers for the TOF measurement. A 2-inch wide photomultiplier tube was attached at both sides of the scintillator. Two 50 μm-thick 16 strip silicon detectors with 5 × 5 cm^2 areas were installed in both the F2 and F3 chambers. All detectors can be moved up and down inside the vacuum chamber by pneumatic actuators. Fig. 6 is a photograph of inside of the F3 chamber, showing the small PPAC, plastic detector, and silicon detector.

Performance of a prototype for PPAC with 20 × 20 cm^2 active area was tested using 3 MeV/nucleon ^{12}C and ^{16}O beams at Kyushu University tandem accelerator laboratory, as described in Ref. [24]. A position resolution of about 0.8 mm in full width at half maximum (FWHM), and a detection efficiency of 94% were measured with an incident beam intensity of 2 × 10^6 particles per second, satisfying the design requirements.

All detectors were tested using a standard ^{241}Am α-source, from which the position, the timing, and the energy resolutions were determined. The position resolution of the PPAC is about 0.8 mm in FWHM with 10 Torr of C_4H_{10} gas. The timing resolution of the plastic detector was measured to be about 0.1 nsec in FWHM. The energy resolution of the silicon detector was determined to be about 1.6% in FWHM from α-particle energy measurements.

6. α-particle transport in KoBRA

We performed an α-particle transport test in KoBRA using a standard ^{241}Am α-source. The ^{241}Am α-source with an active area of 5 mm in diameter was mounted at the production target position F0, and aligned with a tolerance of less than about 0.5 mm. The main α-emissions from ^{241}Am at 5.486 MeV (84.8%), 5.443 MeV (13.1%), and 5.388 MeV (1.66%) were detected and position measurement was made with the large PPAC located at the dispersive focus F1. The α particle was transported from F0 to the F3 chamber, and the position distribution of the α particle was measured using the small PPAC placed at the double achromatic focus F3.

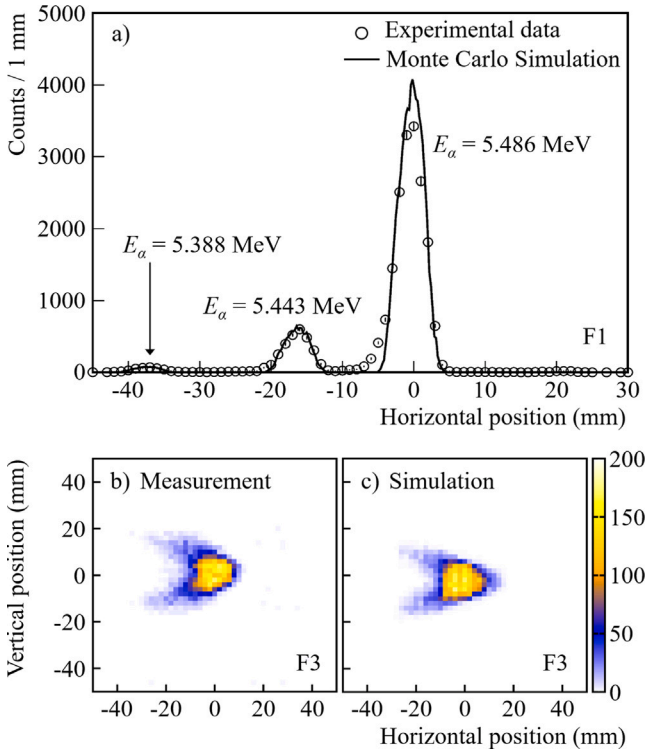

Fig. 7. (a) Position distribution of the α particles at F1. The solid line represents the simulated position distribution normalized to the experimental yield of the alpha particles. (b) Measured position distribution at F3. (c) Simulated position distribution at F3, which was normalized to the experimental yield of the α particles.

The position distribution of the α particles at F1 is shown in Fig. 7(a) with statistical errors. Two peaks are clearly visible at around 0 and −16 mm, which correspond to the α-particle energies (E_α) of 5.486 and 5.443 MeV, respectively. A small peak of α particle of E_α = 5.388 MeV is also shown at −36mm.

The momentum dispersion, D_p, at F1 can be deduced from the following equation:

$$D_p = \frac{d}{(B\rho_1 - B\rho_2)/B\rho_1}\ , \tag{1}$$

where d is the position distance between the peaks at 5.486 and 5.443 MeV in Fig. 7(a). $B\rho_1$ and $B\rho_2$ are the magnetic rigidities of the α particles for E_α = 5.486 and 5.443 MeV, respectively. The distance d was determined to be 16.07 mm by fitting two Gaussian functions. The $B\rho_1$ and $B\rho_2$ were calculated to be 0.33741 and 0.33608 Tm, respectively, from which the dispersion was deduced to be D_p = 4.08 ± 0.03 m, confirming agreement with the design. The quoted error comes from the uncertainty in the fitting. The solid line of Fig. 7(a) represents the results of a Monte Carlo simulation with the code LISE^{++} [26] taking into account the geometry of KoBRA, the detector resolutions, and the fifth order transfer matrix elements, which is consistent with the measured distribution. In the simulation we assumed that ^{241}Am is homogeneously distributed on a disk of diameter 5 mm.

Fig. 7(b) shows the two dimensional position distribution measured at F3. The distribution of Fig. 7(c) was obtained from the same Monte Carlo simulation used for Fig. 7(a). The non-elliptical shape of the position distribution is mainly due to spherical aberrations caused by the large angular distribution of the α particles. The two dimensional position distributions of Fig. 7(b) and (c) are consistent with each other, which evidence that the α particles were successfully transported from F0 to F3 in KoBRA.

7. Summary

In summary, we have constructed KoBRA for low-energy nuclear physics experiments. KoBRA was fabricated and installed in the experimental hall of RAON without the Wien filter. The construction of the Wien filter will be completed by 2024. The momentum dispersion of KoBRA was experimentally determined to be 4.08 ± 0.03 m with an ^{241}Am α-source, confirming the design parameter. The results of α-particle transport are indicative of successful ion transport.

KoBRA will produce RI beams using a primary ^{40}Ar beam at about 25 MeV/nucleon with a graphite production target during the first beam commissioning. In addition, we also have a plan to design a further extension of KoBRA, as reported in Ref. [1]. We expect that KoBRA will provide an opportunity to study the nuclear structure of exotic nuclei and astrophysically interesting nuclear reactions.

Declaration of competing interest

The authors declare that they have no known competing financial interests or personal relationships that could have appeared to influence the work reported in this paper.

Acknowledgments

We would like to thank the administration division staff of RAON for their thoughtful support in the installation of KoBRA. This work was supported by the Rare Isotope Science Project of the Institute for Basic Science funded by Ministry of Science and ICT and NRF of Republic of Korea (2013M7A1A1075764).

References

[1] K. Tshoo, et al., Nucl. Instrum. Methods Phys. Res. B 376 (2016) 188.
[2] Baseline design summary, rare isotope science project, 2012.
[3] Y.K. Kwon, et al., Few-Body Syst. 54 (2013) 961.
[4] D. Jeon, et al., J. Korean Phys. Soc. 65 (2014) 1010.
[5] M. Kwon, et al., J. Part. Accel. Soc. Jpn. 17 (2020) 293.
[6] Y. Chung, H. Kim, M. Kwon, J. Korean Phys. Soc. 80 (2022) 693.
[7] K. Tshoo, Y.K. Kim, et al., Nucl. Instrum. Methods Phys. Res. B 317 (2013) 242.
[8] C.-B. Moon, AIP Adv. 4 (2014) 041001.
[9] B. Hong, JPS Conf. Proc. 1 (2014) 013027.
[10] S. Jeong, et al., J. Korean Phys. Soc. 73 (2018) 516.
[11] J.W. Hwang, et al., Nucl. Instrum. Methods Phys. Res. B 541 (2023) 1.
[12] G.A. Souliotis, et al., Phys. Lett. B 543 (2002) 163.
[13] G.A. Souliotis, et al., Phys. Rev. Lett. 91 (2003) 022701.
[14] G.A. Souliotis, et al., Phys. Rev. C 84 (2011) 064607.
[15] P.N. Fountas, et al., Phys. Rev. C 90 (2014) 064613.
[16] K. Makino, M. Berz, Nucl. Instrum. Methods Phys. Res. B 558 (2006) 346.
[17] H. Takeda, et al., Nucl. Instrum. Methods Phys. Res. B 317 (2013) 798.
[18] T. Uesaka, et al., Nucl. Instrum. Methods Phys. Res. B 266 (2008) 4218.
[19] T. Uesaka, et al., CNS Annual Report, 2005.
[20] T. Uesaka, et al., CNS Annual Report, 2006.
[21] G.P.A. Berg, et al., Nucl. Instrum. Methods Phys. Res. B 376 (2016) 165.
[22] G.P.A. Berg, et al., Nucl. Instrum. Methods A 877 (2018) 87.
[23] W. Rogowski, Arch. Elektrotech. 12 (1923) 1.
[24] C. Akers, et al., Nucl. Instrum. Methods A 910 (2018) 49.
[25] C. Akers, et al., J. Korean Phys. Soc. 70 (2017) 682.
[26] O.B. Tarasov, D. Bazin, Nucl. Instrum. Methods Phys. Res. B 376 (2016) 185.